The problem of complex shape tracking in a Campbell Diagram or how to overcome crossing/veering phenomena

Guillaume Mogenier, Thouraya Baranger, Guy Ferraris, Régis Dufour, Lionel Durantay

The problem of complex shape tracking in a Campbell Diagram or how to overcome crossing/veering phenomena

G. Mogenier[a], T. Baranger[a,b], G. Ferraris[a], R. Dufour[a], L. Durantay[c]
[a]Université de Lyon, CNRS, INSA-Lyon, LaMCoS UMR5259, France
[b]Université Lyon, CNRS, Université Lyon 1, LaMCoS UMR5259, France
[a]Converteam SAS, Rotating Machines Division, France

ABSTRACT

The correlation criterion proposed in this article and called NC^{2}O (Normalized Cross Complex Orthogonality) ensures bi-orthogonality properties between rotor mode shapes calculated at different speeds of rotation. This criterion is proofed on an industrial laminated rotor composed of disks and two fluid film bearings, whose stiffness and damping characteristics depend on the speed of rotation. The industrial finite element model shows that the NC^{2}O criterion provides a more efficient mode pairing of rotor shapes than those obtained by using the classical correlation criteria. Moreover this criterion maker easier the Campbell diagram plotting of strongly $\dot{\phi}$-dependent structures.

1 INTRODUCTION

Predicting the lateral dynamics of industrial rotating machines is a common task for several decades and a lot of reference books can be cited, see for example [1, 2, 3, 4]. In addition to natural frequencies, the main objective of such predictions is stress field distributions, a decisive step in the design process of both rotating machine or not. Thus estimating deformed shapes is an efficient way that provides qualitatively stress field distributions. Therefore informations related to deformed shapes, *i.e.* mode shapes, make sense especially in frequency domain responses. However, when dealing with rotating machines, gyroscopic effect induces the well-known dependence of natural frequencies and associated mode shapes with respect to the speed of rotation, a dependence most of the times enhanced by bearing characteristics. It involves an often encountered problem in Campbell diagram plotting because, at each speed of rotation, the eigenvalue problem solver classically provides natural frequencies sorted in ascending order whereas mode shapes can switch their orders. Consequently being able to know which mode shape is associated with the k^{th} natural frequency at a speed of rotation does not ensure that this shape corresponds to the k^{th} natural frequency at another speed. Thereby this complexity of gyroscopic systems emanates from veering or crossing phenomena which make difficult the tracking of rotor shapes versus the speed of rotation and thus determining which mode shape is excited.

The so-called mode pairing may overcome the latter problem by correlating two sets of mode shapes. In this way, several correlation criteria have been developed for the last thirty years. They consist in filled matrices with terms between zero and one, the latter indicates a perfect correlation while zero stands for a poor one. The most popular is certainly the MAC (Modal Assurance Criterion), introduced in [5], which was tried and tested in model updating to correlate numerical and experimental mode shapes [6, 7, 8, 9]. Other criteria using stiffness or mass matrices have been later established to estimate besides orthogonality between compared mode shapes such as the NCO (Normalized Cross Orthogonality) [10, 11]. In [12], an automatic mode pairing strategy

is suggested by using a criterion based on combination of the MAC and modal strain energies. The IERI criterion used in [13] estimates rather correlation between mode shape difference. Unlike the MAC, those are well adapted to correlate real mode shapes because they ensure collinearity and overall orthogonality with respect to structural matrices, as introduced by modal theory. Furthermore orthogonality guarantee is a powerful concept which implies so small correlation terms even if mode shapes seem to be close. These terms, reaching zero, greatly facilitate the pairing of shapes whose corresponding terms are usually close to unity. Nevertheless some authors still prefer the MAC when dealing with pairing of real shapes of parametric systems subjected to veering or crossing phenomena such as in [14] regarding mode shapes of a constrained eigenvalue problem of a cracked plate. In the same manner, although authors of [15] had noticed that off-diagonal terms of the MAC were of order of 0.4, they did not decide to benefit from orthogonality properties of eigenvectors of the prestressed truss they studied. Contrary to [16], in which criteria are established to distinguish veerings from crossings, the present paper rather intend to provide an efficient criterion for pairing complex mode shapes and tracking any shape needed, especially for finite element model of complex damped gyroscopic structures without analytical solutions.

This paper presents a new correlation criterion called NC^{2}O (Normalized Cross Complex Orthogonality) which ensures orthogonality properties between rotor mode shapes calculated at different speeds of rotation $\dot{\phi}$. Indeed the quadratic and non symmetric natures of the related eigenvalue problem involve complex eigenvectors which do not satisfy the same properties profited by the previous criteria. Therefore applying them to rotor mode shapes does not take advantage of orthogonality properties in the mode pairing process. Motion equations of damped gyroscopic structures are presented as well as associated quadratic eigenvalue problem. After reminding the bi-orthogonality properties of complex mode shapes, the NC^{2}O criterion is developed. Finally, it is proofed on a finite element model of an industrial laminated rotor composed of disks and two fluid film bearings whose stiffness and damping are clearly $\dot{\phi}$-dependent. This can show that NC^{2}O provides a more efficient mode pairing of rotor shapes than those obtained by using classical correlation criteria, especially for Campbell diagram plotting of strongly $\dot{\phi}$-dependent structures.

2 BACKGROUND EQUATIONS

The steady-state dynamic behavior of a discretized damped gyroscopic structure is governed by the set of n_δ equations:

$$M\ddot{\delta}(t) + C\left(\dot{\phi}\right)\dot{\delta}(t) + K\left(\dot{\phi}\right)\delta(t) = \mathscr{F}(t), \tag{1}$$

with $\delta(t)$ the generalized displacements vector while $\dot{(\,)}$ stands for derivative with respect to time t. The mass matrix is denoted by M whereas K, C matrices represent stiffness, viscous damping as well as gyroscopic effect respectively, both of them including $\dot{\phi}$-dependent fluid film bearing characteristics. $\mathscr{F}(t)$ is the external force vector.

2.1 Complex eigenelements of rotors

The first step of a dynamic analysis consists in solving the homogeneous Eq. (1) at a given speed $\dot{\phi}$ such as:

$$M\ddot{\delta}(t) + C\left(\dot{\phi}\right)\dot{\delta}(t) + K\left(\dot{\phi}\right)\delta(t) = 0. \tag{2}$$

Introducing the general solution $\delta(t) = \Psi_k e^{\lambda_k t}$ in Eq. (2) involves the following eigenvalue problem:

$$\left[\lambda_k^2 M + \lambda_k C\left(\dot{\phi}\right) + K\left(\dot{\phi}\right)\right]\Psi_k = 0, \tag{3}$$

whose quadratic nature involves $k = 1, \ldots, n_\delta$ couples of complex conjugate eigenvalues and right eigenvectors denoted by λ_k and Ψ_k respectively. In addition, by adding a trivial identity of order n_δ, [17, 18]:

$$M\dot{\delta}(t) - M\dot{\delta}(t) = 0, \tag{4}$$

the quadratic problem can be written in a more convenient $2n_\delta$ order linear form, *i.e.* by introducing a state space representation of Eq. (2) described with the state vector $y(t)$ including displacements and speeds [19, 20]:

$$A\dot{y}(t) - By(t) = 0 \quad \text{with} \quad y(t) = \left(\dot{\delta}(t),\ \delta(t)\right)^t, \tag{5}$$

with $(\ )^t$ the transpose operator and the augmented matrices $A,\ B$ defined by:

$$A = \begin{bmatrix} 0 & M \\ M & C(\dot{\phi}) \end{bmatrix}, \tag{6a}$$

$$B = \begin{bmatrix} M & 0 \\ 0 & -K(\dot{\phi}) \end{bmatrix}. \tag{6b}$$

Considering the general solution $y(t) = {}^r\Upsilon_k e^{\lambda_k t}$ of Eq. (5) and the unsymmetric nature of matrices A, B, the state space problem admits a generalized eigenproblem (7a) and an associated dual one (7b) with the same eigenvalues:

$$B^r\Upsilon = \Lambda A^r\Upsilon, \tag{7a}$$

$$B^{tl}\Upsilon = \Lambda A^{tl}\Upsilon, \tag{7b}$$

where ${}^r\Upsilon,\ {}^l\Upsilon$ denotes the right and left eigenvector matrices of the state space system respectively, whose k^{th} columns hold:

$${}^r\Upsilon_k = (\lambda_k\Psi_k,\ \Psi_k)^t, \tag{8a}$$

$${}^l\Upsilon_k = (\lambda_k\Theta_k,\ \Theta_k)^t, \tag{8b}$$

with Θ_k the k^{th} left eigenvector of Eq. (2) and Λ contains the n_δ couples of complex conjugate eigenvalues $\{\lambda_k,\ \lambda_k^*\}$ as a function of the natural frequency ω_k and modal damping factor ξ_k deduced by:

$$\omega_k = \frac{1}{2}j\left(\lambda_k^* - \lambda_k\right), \tag{9a}$$

$$\xi_k^2 = \frac{1}{2}\left(1 + \frac{\lambda_k^*}{\lambda_k}\right), \tag{9b}$$

with $j^2 = -1$ and $(\ )^*$ the complex conjugate operator.

Thus natural frequencies enable to plot the Campbell diagram and determine critical speeds.

2.2 Dual-orthogonality properties

Let $\{\lambda_k, {}^r\Upsilon_k\}$, $\{\lambda_q, {}^l\Upsilon_q\}$ be distinct right and left eigenelements of Eq. (7). Premultiplying Eqs. (7a) and (7b) by ${}^l\Upsilon_q^t$ and ${}^r\Upsilon_k^t$ respectively leads to:

$${}^l\Upsilon_q^t B^r\Upsilon_k = \lambda_k\,{}^l\Upsilon_q^t A^r\Upsilon_k, \tag{10a}$$

$${}^r\Upsilon_k^t B^{tl}\Upsilon_q = \lambda_q\,{}^r\Upsilon_k^t A^{tl}\Upsilon_q. \tag{10b}$$

The transposition of Eq. (10b) gives:

$${}^l\Upsilon_q^t B^r\Upsilon_k = \lambda_q\,{}^l\Upsilon_q^t A^r\Upsilon_k. \tag{11}$$

Subtracting Eq. (10a) and (11) yields the equality:

$$(\lambda_q - \lambda_k)\,{}^l\Upsilon_q^t A^r\Upsilon_k = 0 \iff {}^l\Upsilon_q^t A^r\Upsilon_k = 0 \quad \forall q \neq k, \tag{12}$$

since $\lambda_k \neq \lambda_q$. Introducing Eq. (12) in (10a) gives the second relation. Thus bi-orthogonality properties of left and right eigenvectors with respect to augmented matrices, [21, 22], satisfy:

$${}^l\Upsilon_q^t A^r\Upsilon_k = \alpha_{qk}\delta_{qk}, \tag{13a}$$

$${}^l\Upsilon_q^t B^r\Upsilon_k = \beta_{qk}\delta_{qk}, \tag{13b}$$

with $\alpha_{qk}, \beta_{qk} \in \mathbb{C}$ and δ_{qk} the Kronecker symbol.

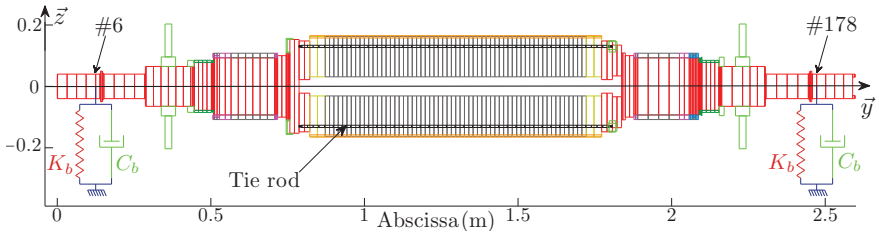

Figure 1: Branched finite element model of the industrial rotor.

Finally, right and left eigenvectors $\{\Psi_k,\ \Theta_k\}$ and bi-orthogonality properties defined in Eqs. (13) permit uncoupling and solving Eq. (1) while reducing CPU-time.

3 A NEW CRITERION FOR ROTOR MODE SHAPE TRACKING

Equation (2) is solved for each $\dot{\phi}_i$, $i = 1 \dots n_{\dot{\phi}}$ and provides the sets of the first m sorted natural frequencies ω^i in ascending order, and associated right Ψ^i and left Θ^i mode shapes; the upperscript stands for the i^{th} speed. Note that Campbell diagram has to illustrate the evolution of the natural frequency ω_{Ψ_k} related to its own mode shapes Ψ_k and not the ascending sorted ω_k. Then defining a criterion, that identifies which shape Ψ_k^i is related to ω_q^i, is required since the inequality $q \neq k$ frequently holds true if crossings occur, *i.e.* when Ψ_k^i associated with ω_k^i does not correspond to Ψ_k^{i+1} related to ω_k^{i+1}.
Equation (13b) can be expressed as follows:

$$(\lambda_q \Theta_q,\ \Theta_q)^t \begin{bmatrix} M & 0 \\ 0 & -K\left(\dot{\phi}\right) \end{bmatrix} \begin{pmatrix} \lambda_k \Psi_k \\ \Psi_k \end{pmatrix} = \delta_{qk} \beta_{qk}, \tag{14}$$

and expanded such as:

$$\Theta_q^t \left[\lambda_q \lambda_k M - K\left(\dot{\phi}\right)\right] \Psi_k = \delta_{qk} \beta_{qk}. \tag{15}$$

Thus developing an efficient correlation indicator, which takes advantage of bi-orthogonality properties of Eq. (15), is feasible and could have the following expression:

$$\text{NC}^2\text{O}_{k,q} = \delta_{qk} \frac{\left|\beta_{qk}\right|^2}{\left|\beta_{qq}\right| \cdot \left|\beta_{kk}\right|} = \begin{cases} 0 & \text{if} \quad k \neq q \\ 1 & \text{if} \quad k = q \end{cases}, \tag{16}$$

with $|\ |$ the modulus operator. We suggested to call this criterion NC^{2}O (Normalized Cross Complex Orthogonality) as an extension of NCO applied to damped gyroscopic structures. Thus in a complex mode pairing strategy related to Campbell diagram, we consider two sets of eigenelements at both $\dot{\phi}_i$ and $\dot{\phi}_{i+1}$ such as NC^{2}O takes the form:

$$\text{NC}^2\text{O}_{k,q}^{i,i+1} = \frac{\left|\mathscr{L}_q^{i+1} \mathscr{W}_{k,q}^{i,i+1} \mathscr{R}_k^i\right|^2}{\left|\mathscr{L}_q^{i+1} \mathscr{W}_{q,q}^{i+1,i+1} \mathscr{R}_q^{i+1}\right| \cdot \left|\mathscr{L}_k^i \mathscr{W}_{k,k}^{i,i} \mathscr{R}_k^i\right|}, \tag{17}$$

where row and column indexes $k,\ q$ are related to shapes, at $\dot{\phi}_i$, $\dot{\phi}_{i+1}$, and assuming the following correspondences:

$$\mathscr{L} \equiv \Theta^t, \tag{18a}$$

$$\mathscr{R} \equiv \Psi. \tag{18b}$$

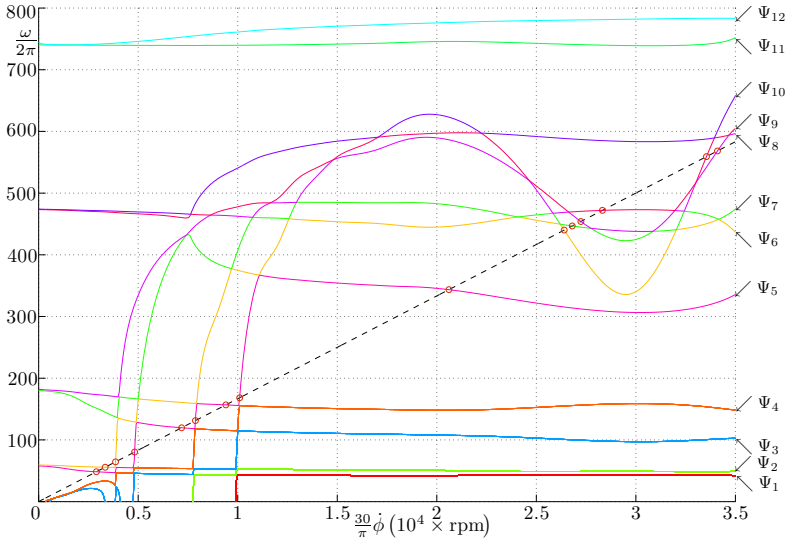

Figure 2: Campbell diagram without mode pairing. Natural frequencies are plotted in Hz. Circles (○) and dashed line (−−) indicate critical speeds and 1 × excitation respectively.

The weighting matrix $\mathscr{W}_{k,q}^{i,+1}$ is defined by:

$$\mathscr{W}_{k,q}^{i,i+1} = \lambda_k^i \lambda_q^{i+1} M - K\left(\dot{\phi}_i\right), \tag{19}$$

Remark: NC^{2}O can be applied to damped gyroscopic structures reduced in the modal basis of the undamped and non-rotating associated structure [3]. So modal matrices and associated eigenelements have to be used in Eq. (17).

4 INDUSTRIAL APPLICATION

4.1 Finite element model

The industrial application consists in a induction rotor made of prestressed laminated stack with tie rods as presented in [23, 24]. Total mass and length are $1\ 026$ kg and 2.6 m. By coupling Timoshenko theory [25] and Euler angles ψ, θ, ϕ, *i.e.* precession, nutation and intrinsic rotation roughly around $\vec{z}$, $\vec{x}$ and $\vec{y}$ respectively, the rotor is discretized in $N_e = 239$ two node elements ($n_\delta = 956$ dof), all of them containing eight dof stored in ${}^e\delta$ such as:

$${}^e\delta = \left(w_e, u_e, \psi_e, \theta_e, w_{e+1}, u_{e+1}, \psi_{e+1}, \theta_{e+1}\right)^t, \tag{20}$$

with u, w lateral dof along $\vec{x}$, $\vec{z}$ respectively while ψ, θ stand for associated rotations around $\vec{z}$ and $\vec{x}$. It is assumed that the rotor is supported by two identical fluid film bearings located at nodes $\#6$ and $\#178$, Fig. 1. Bearing characteristics are given by Figs. 8(a) and 8(b) for the $\left[0, 3.5 \cdot 10^4\right]$ rpm speed range. Thus both steel disks mounted on shaft-ends as well as bearing stiffnesses and dampings should induce a strongly gyroscopic/$\dot{\phi}$-dependent dynamic behavior of the rotor.

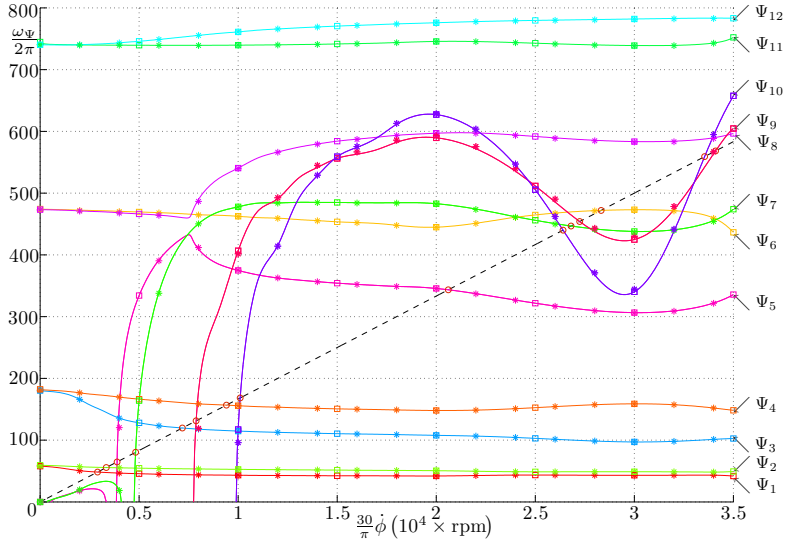

Figure 3: Campbell diagram using the NC^{2}O mode pairing for different $\dot{\phi}$-steps: $5 \cdot 10^1$ (–), $2 \cdot 10^3$ (∗) and $5 \cdot 10^3$ rpm (□).

4.2 Campbell diagram calculation

Natural frequencies and complex mode shapes are obtained by solving Eqs. (7), at each constant speed $\dot{\phi}_i$. For the sake of matrix reduction, the pseudo-modal method is preferred [3] by projecting Eq. (2) in non-rotating modal basis containing $m = 12$ mode shapes. Besides reducing CPU-time, that enables also modal damping factors introduction, *e.g.* 1%. Moreover the variability of bearing characteristics involves the calculation of a new modal basis $\Phi\left(\dot{\phi}_i\right)$ at each $\dot{\phi}_i$, by solving the eigenvalue problem:

$$K\left(\dot{\phi}_i\right)\Phi\left(\dot{\phi}_i\right) = \Lambda_0 M \Phi\left(\dot{\phi}_i\right), \tag{21}$$

with Λ_0 containing undamped eigenvalues, at rest.

By setting the step of speed of rotation at 50 rpm, a first Campbell diagram is illustrated by Fig. 2 as the evolution of the first m natural frequencies ω sorted in ascending order, *i.e* without using any mode pairing process. On the other hand, Fig. 3 presents the Campbell diagram which benefits from mode pairing process, especially the one using the NC^{2}O criterion. It should be noted that complex shapes are arbitrarily indexed, at the upper bound $\dot{\phi}_{n_{\dot{\phi}}}$, by associating them with indexes of corresponding sorted natural frequencies in ascending order. Actually, the Campbell diagram shows several crossing and veering phenomena and it may be stated that each natural frequency crosses one of the other one the in considered speed range, Fig. 4. Indeed one veering occurrence clearly appears between complex shapes Ψ_5 and Ψ_8 around $7.5 \cdot 10^3$ rpm. Furthermore it may be counted no less than 56 crossing occurrences between all the first m natural frequencies which brings out the strongly $\dot{\phi}$-dependent behavior of the supported rotor.

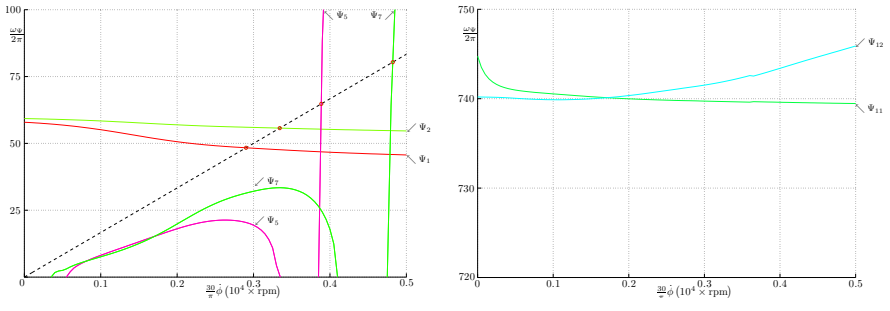

(a) (b)

Figure 4: Enlarging of Campbell diagram emphasizing crossing phenomena between: $\Psi_{1,2,5}$ and Ψ_7, (a) Ψ_{11} and Ψ_{12} (b) .

5 OVERCOMING VEERING/CROSSING PHENOMENA

To proof the NC^{2}O criterion, Fig. 3 presents star and square symbols which correspond to Campbell diagrams obtained with speed of rotation steps of $2 \cdot 10^3$ rpm and $5 \cdot 10^3$ rpm respectively. Although latter steps are larger than the initial one (continuous lines), all Campbell diagrams coincide together whatever step lengths and crossings or veerings , *e.g.* it could be cited the 9^{th} or 10^{th} complex shapes for which 13 or 16 crossing occurrences appear respectively. Thereof that underlines the efficiency of NC^{2}O criterion in mode paring process, which provides Campbell diagrams allowing any mode shape tracking. In addition, Fig. 5 presents the following quantities:

$$\text{NC}^2\text{O}_\perp = \sum_{\substack{k,q=1 \\ q \neq k}}^{m} \frac{\text{NC}^2\text{O}_{k,q}^{i,i+1}}{m\,(m-1)}, \qquad (22a) \qquad \text{MAC}_\perp = \sum_{\substack{k,q=1 \\ q \neq k}}^{m} \frac{\text{MAC}_{k,q}^{i,i+1}}{m\,(m-1)}. \qquad (22b)$$

$$\text{NCO}_{\text{K}_\perp} = \sum_{\substack{k,q=1 \\ q \neq k}}^{m} \frac{\text{NCO}_{\text{K}_{k,q}}^{i,i+1}}{m\,(m-1)}, \qquad (23a) \qquad \text{NCO}_{\text{M}_\perp} = \sum_{\substack{k,q=1 \\ q \neq k}}^{m} \frac{\text{NCO}_{\text{M}_{k,q}}^{i,i+1}}{m\,(m-1)}. \qquad (23b)$$

as averages of off-diagonal terms of well-known correlation criteria listed in Table 1. Figure 5 underlines the difference of order of magnitude between off-diagonal terms of the NC^{2}O and the other criteria evaluated at speeds $\dot{\phi}_i$, $\dot{\phi}_{i+1}$, $i = 1, \ldots, n_{\dot{\phi}} - 1$ regarding the Campbell diagram shown in Fig. 3. The MAC off-diagonal terms are of order of 10^{-1} while those related the NCO calculated either with the mass or stiffness matrices are rather of order of 10^{-2}. Nevertheless there is a significant difference by comparison with those provides by NC^{2}O which are mainly of order of 10^{-6} and reach 10^{-8}.

As a result, small terms greatly facilitate the pairing process, and also argues for using a correlation criterion based on bi-orthogonality properties. As previously mentioned, several crossing occurrences appear between the first m natural frequencies ω_Ψ in the speed range. It can be stated that ω_{Ψ_9} and $\omega_{\Psi_{10}}$ cross 13 and 16 times other natural frequencies respectively. Figure 6 presents a zoom in of Fig. 3 between $\dot{\phi}_i = 9 \cdot 10^3$ rpm and $\dot{\phi}_{i+1} = 1.2 \cdot 10^4$ rpm while Figs. 7(a) to 7(d) represent the NC^{2}O, MAC, NCO$_\text{K}$ and NCO$_\text{M}$ correlation matrices respectively. Even if

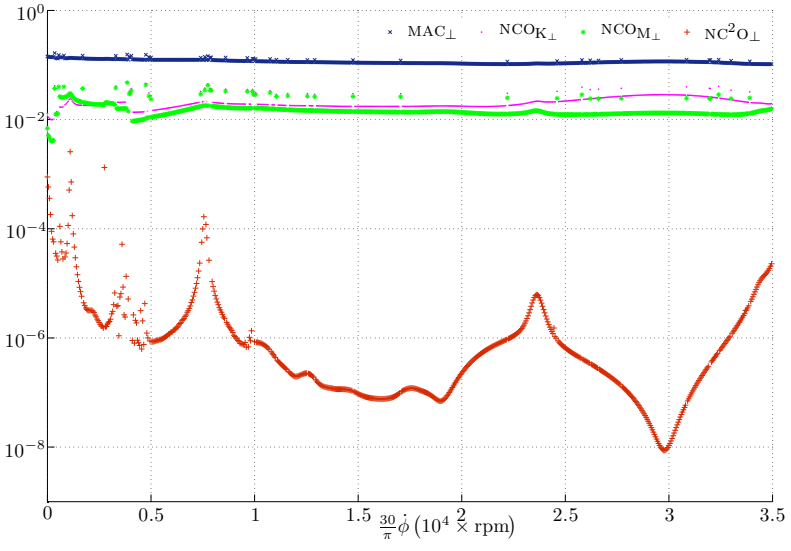

Figure 5: Off-diagonal term averages of MAC$_\perp$ ($\times$), NCO$_{K_\perp}$ ($\bullet$), NCO$_{M_\perp}$ ($*$) and NC^{2}O$_\perp$ ($+$) correlation criteria.

correlation criteria were calculated between speeds far from the one at which the veering occurs, the MAC suggest one more time a virtual correlation between the shapes subjected to veering and associated to ω_{Ψ_5} and ω_{Ψ_8}, *i.e.* the 7^{th} and 10^{th} mode shapes Ψ_7^i, Ψ_{10}^i calculated at $\dot{\phi}_i$ and the 10^{th} and 5^{th} shapes Ψ_{10}^{i+1} , Ψ_5^{i+1} calculated at $\dot{\phi}_{i+1}$.

Indeed non-correspondence terms of the MAC are higher than 10^{-1} (0.7) whereas both NCO$_K$ and NCO$_M$ provide terms of order of 0.5. In addition to the fact that NC^{2}O is not disturbed by high value terms, and although being evaluated between speeds spaced out over $3 \cdot 10^3$ rpm, Fig. 7(a) gives well correspondences between complex shapes of the $\dot{\phi}$-interval bounds, and is then in good agreement with Fig. 6. Finally the NC^{2}O criterion presents a typically binary behavior due to Kronecker symbol of Eq. (16), *i.e.* two sets of non-coincident eigenelements involves terms almost null. Furthermore it has been stated that crossing phenomena are clearly observed and distinguished by the NC^{2}O, the latter being set without any disturbed terms values as doubloons or artefacts significantly higher than zero as it appears in the MAC, Fig. 7(b). Consequently, NC^{2}O does not present any drawbacks of the other criteria and comprise an efficient criterion either to pair complex shape bases or track any complex shape, especially in Campbell diagram cases.

Table 1: Correspondences between correlation criteria

Criterion	NC^{2}O$_{k,q}^{i,i+1}$	MAC$_{k,q}^{i,i+1}$	NCO$_{K_{k,q}}^{i,i+1}$	NCO$_{M_{k,q}}^{i,i+1}$
$\mathscr{L}_q^{i+1}$	$\Theta_q^{t\,i+1}$	$\Psi_q^{*t\,i+1}$	$\Psi_q^{*t\,i+1}$	$\Psi_q^{*t\,i+1}$
$\mathscr{W}_{k,q}^{i,i+1}$	$\lambda_k^i \lambda_q^{i+1} M - K\left(\dot{\phi}_i\right)$	I	$K\left(\dot{\phi}_i\right)$	M
$\mathscr{R}_k^i$	Ψ_k^i	Ψ_k^i	Ψ_k^i	Ψ_k^i

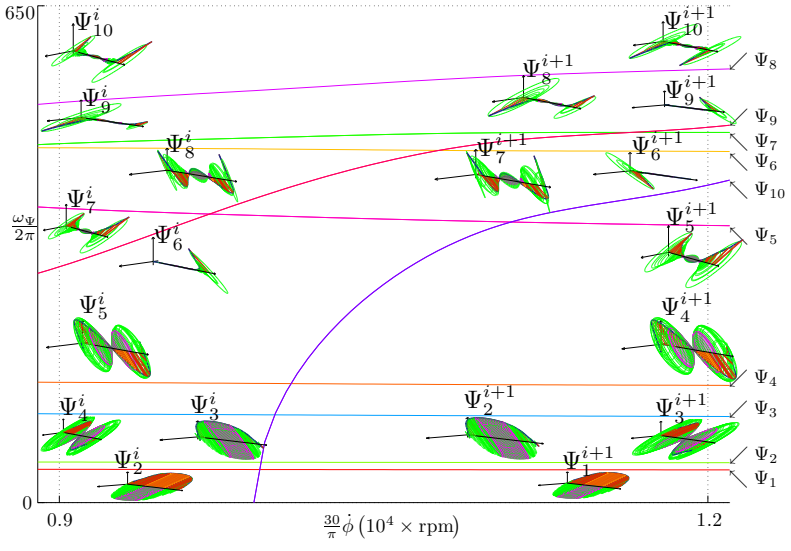

Figure 6: Crossing phenomena between $9 \cdot 10^3$ and $1.2 \cdot 10^4$ rpm.

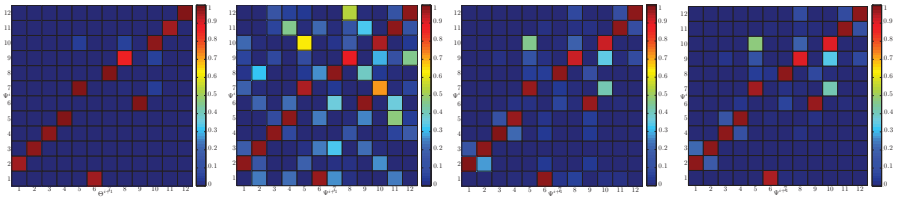

(a) **NC^{2}O.** (b) **MAC.** (c) **NCO$_K$.** (d) **NCO$_M$.**

Figure 7: Criteria calculated between $9 \cdot 10^3$ and $1.2 \cdot 10^4$ rpm.

6 CONCLUSION

The correlation criterion proposed is based on the bi-orthogonality properties of right and left eigenvectors of damped gyroscopic structures. The NC^{2}O criterion greatly facilitates the rotor mode shapes pairing even if veering or crossing phenomena occur. Thus Campbell diagrams can be plotted by illustrating the evolution of each natural frequency associated with its own complex mode shape in the speed of rotation range. Finally the industrial application, whose bearings' characteristics strongly depend on the speed of rotation, proofed the efficiency of the NC^{2}O in the mode pairing process.

7 REFERENCE LIST

[1] Dimentberg, F., 1961. *Flexural vibrations of rotating shafts*. Butterworths'.

[2] Lee, C., 1993. *Vibration analysis of rotors*. Springer.

[3] Lalanne, M., and Ferraris, G., 1998. *Rotordynamics Prediction in Engineering*, 2^{nd} ed. John Wiley $\&$ Sons Ltd, New York.

[4] Genta, G., 2005. *Dynamics of rotating systems*, 1^{st} ed. Springer Verlag, New York.

[5] Allemang, R., and Brown, D., 1982. "A correlation coefficient for modal vector analysis". In Proceedings of the International Modal Analysis Conference & Exhibit (1982), pp. 110–116.

[6] Ewins, D., 1984. *Modal Testing: Theory and Practice*. Research Studies Press LTD., England.

[7] Heylen, W., and Janter, T., 1990. "Extensions of the modal assurance criterion". *Journal of vibration, acoustics, stress, and reliability in design,* **112**(4), pp. 468–472.

[8] Ting, T., Chen, T., and Twomey, W., 1993. "Correlating modes shapes based on the modal assurance criterion". *Finite Elements in Analysis and Design,* **14**(4), pp. 353–360.

[9] Blaschke, P., and Ewins, D., 1997. "The MAC revisited and updated". In Proceedings of SPIE, the International Society for Optical Engineering (1997), Vol. 3089, pp. 147–154.

[10] Lieven, N., 1994. "Error location using normalised orthogonality". In International Modal Analysis Conference (IMAC), 12 th, Honolulu, HI (1994), pp. 761–764.

[11] Morales, C., 2005. "Comments on the MAC and the NCO, and a linear modal correlation coefficient". *Journal of Sound and Vibration,* **282**(1-2), pp. 529–537.

[12] Brehm, M., Zabel, V., and Bucher, C., 2010. "An automatic mode pairing strategy using an enhanced modal assurance criterion based on modal strain energies". *Journal of Sound and Vibration,* **329**, pp. 5375–5392.

[13] Bodel, C., 2009. "Opérateur MAC_MODES". *Code_Aster : Fascicule u4.52: Analyse modale,* **U4 52 15**(1647), pp. 1–5.

[14] Saito, A., Castanier, M., and Pierre, C., 2009. "Estimation and veering analysis of nonlinear resonant frequencies of cracked plates". *Journal of Sound and Vibration,* **326**(3-5), pp. 725–739.

[15] Du Bois, J., Adhikari, S., and Lieven, N., 2009. "Eigenvalue curve veering in stressed structures: An experimental study". *Journal of Sound and Vibration,* **322**(4-5), pp. 1117–1124.

[16] Perkins, N., and Mote Jr, C., 1986. "Comments on curve veering in eigenvalue problems". *Journal of Sound and Vibration,* **106**(3), pp. 451–463.

[17] Gmür, T., 1997. *Dynamique des structures: Analyse modale numérique*. Presses Polytechniques et Universitaires Romandes, Lausanne, Suisse.

[18] Bavastri, C., Ferreira, E., Espíndola, J., and Lopes, E., 2008. "Modeling of dynamic rotors with flexible bearings due to the use of viscoelastic materials". *Journal of the Brazilian Society of Mechanical Sciences and Engineering,* **30**, pp. 22–29.

[19] Meirovitch, L., 1974. "A new method of solution of the eigenvalue problem for gyroscopic systems (using state vectors)". In (National Congress of Applied Mechanics, 7 th, Boulder, Colo., June 3-7, 1974.) AIAA Journal„ Vol. 12, pp. 1337–1342.

[20] Khulief, Y., and Mohiuddin, M., 1997. "On the dynamic analysis of rotors using modal reduction". *Finite Elements in Analysis and Design,* **26**(1), pp. 41–55.

[21] Nelson, R., 1976. "Simplified calculation of eigenvector derivatives". *AIAA Journal,* **14**(9), pp. 1201–1205.

[22] Sui, Y., and Zhong, W., 2006. "Eigenvalue problem of a large scale indefinite gyroscopic dynamic system". *Applied Mathematics and Mechanics,* **27**(1), pp. 15–22.

[23] Mogenier, G., Baranger, T., Dufour, R., Durantay, L., and Barras, N., 2011. "Efficient model development for an assembled rotor of an induction motor using a condensed modal functional". *Journal of Computational and Nonlinear Dynamics,* **6**(2), January, pp. 1–8.

[24] Mogenier, G., Baranger, T., Dufour, R., Ferraris, G., and Durantay, L., 2011. "Non linear centrifugal effects on prestressed laminated rotors". *Journal of Mechanism and Machine Theory,* **46**(10), October, pp. 1466–1491.

[25] Przemieniecki, J.-S., 1985. *Theory of Matrix Structural Analysis*, 46^{th} ed. Dover Publications, INC., New York.

A-Bearing Characteristics

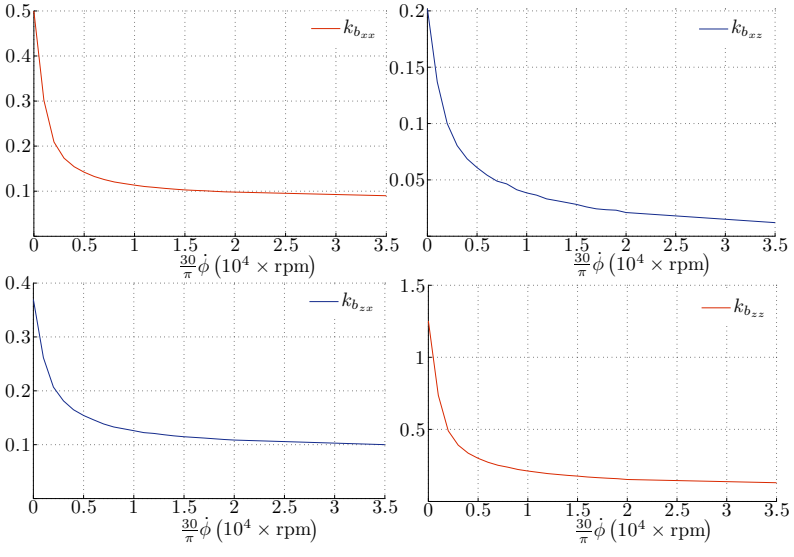

(a) **Stiffness** $\left(10^9 \times \mathrm{N} \cdot \mathrm{m}^{-2}\right)$.

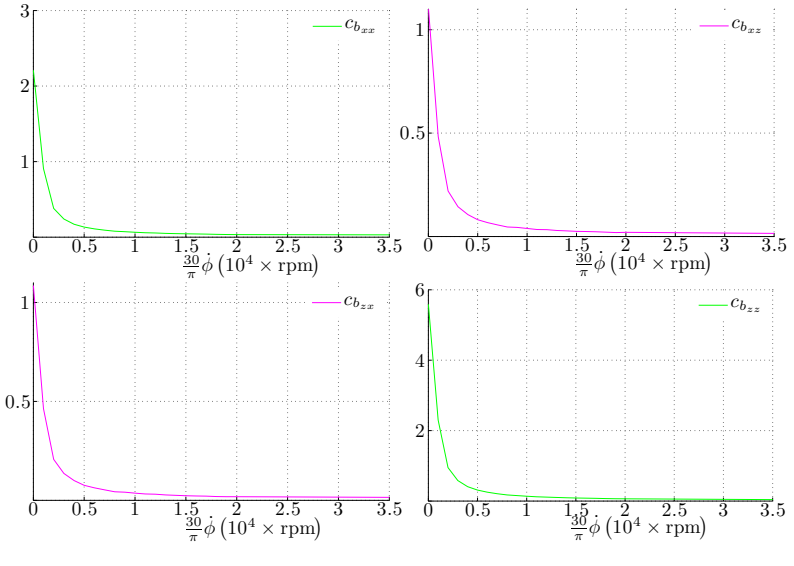

(b) **Damping** $\left(10^6 \times \mathrm{N} \cdot \mathrm{s} \cdot \mathrm{m}^{-1}\right)$.

Figure 8: Hydrodynamic bearings characteristics.